14th European Signal Processing Conference (EUSIPCO 2006), Florence, Italy, September 4-8, 2006, copyright by EURASIP

MULTICHANNEL IMAGE DECONVOLUTION IN THE WAVELET TRANSFORM DOMAIN

A. Benazza-Benyahia[1] , *J.- C. Pesquet*[2]

[1] URISA, SUP'COM
Route de Raoued 3.5 Km, 2083 Ariana, Tunisia
phone: + (216) 71857000, fax: + (216) 71856829, email: ben.yahia@planet.tn

[2] IGM and UMR-CNRS 8049,
Université de Marne-la-Vallée,
Champs-sur-Marne, 77454 Marne-la-Vallée, France
email: pesquet@univ-mlv.fr

ABSTRACT

In this paper, we are interested in restoring blurred multicomponent images corrupted by an additive Gaussian noise. The novelty of the proposed approach is two-fold. Firstly, we show how to combine M-band Wavelet Transforms (WT) with Fourier analysis to restore multicomponent images. Secondly, we point out that the multichannel deconvolution procedure takes advantage of exploiting multivariate regression rules. Simulations experiments carried out on multispectral satellite images indicate the good performance of our method.

1. INTRODUCTION

Satellite imaging systems tend to have increasing spatial and spectral resolutions. Operating in different spectral ranges, these instruments provide several spectral components. Therefore, a multichannel image is delivered for a single sensed area. For instance, for the SPOT5 satellite, the High Resolution Visible imaging on-board systems acquire 4 spectral images XS1, ..., XS4. However, the image sensing stage generally suffers from various types of degradations. The satellite motion coupled with the optics imperfections yield blurred images. Furthermore, these images are corrupted by an additive noise produced by the electronics of the device. These artifacts should be removed prior to fully exploiting the data for further remote sensing tasks. Much attention was paid to both the denoising and the deconvolution problems. It is worth pointing out that two alternatives have been envisaged for multispectral image denoising/restoration. The first one consists of a *separate* processing of the spectral components whereas the second one captures their mutual correlations through a *multichannel* procedure. Concerning the denoising problem, the two alternatives have already been studied. Monochannel methods are often based on spatial filters such as the well-known Wiener filter or order statistic filters [1]. Besides, thanks to the good energy compaction and decorrelation properties of the Wavelet Transform (WT), simple shrinkage operation in the wavelet domain were developped [2]. In the framework of multichannel denoising, we have recently proposed a very efficient and robust method that jointly reduces the noise of the wavelet coefficients of the spectral components [3].
In a similar way, much works have been dedicated to monochannel deconvolution [4, 5, 6]. The multichannel restoration problem have been also extensively studied. Pioneering works attempted to design appropriate filters in the frequency domain [7, 8, 9] . The WT domain was successfully investigated but mainly in the case of *monochannel* deconvolution [10, 11, 12, 13, 14]. A recent attention was recently paid to combine the Meyer two-band WT and the Fourier transform for deconvolution purposes through an elegant and efficient wavelet image deblurring method called Waved. However, to the best of our knowledge, few papers were reported concerning wavelet-based restoration methods for multicomponent images. In this paper, we aim at designing a new multivariate statistical deconvolution technique. The contributions of this paper are the following.

- Firstly, the deconvolution problem is formulated using an arbitrary M-band WT instead of the conventional two-band Meyer case in order to gain more flexibility in the multiresolution analysis.
- Secondly, we extend the Waved method to the multichannel case and propose a multicomponent statistical estimation technique.
- Besides, the calculations are performed for an arbitrary covariance matrix between the multispectral noise components.

The paper is organized as follows. In Section 2, the problem is stated and our notation is introduced. The main properties of periodized Meyer wavelets and M-band decompositions are briefly recalled in Section 3. In Section 4, we present the Waved estimator. In Section 5, we compute explicit expressions of the statistics of the Waved estimator. In Section 6, we describe an extension of the Waved method to the case of multicomponent data. In Section 7, some experimental results are provided to evaluate the performance achieved by our multivariate estimation approach and, some concluding remarks are also given in Section 8. Throughout the paper, the following notation will be used: let M be an integer greater than or equal to 2, $\mathbb{N}_M = \{0,\dots,M-1\}$ and $\mathbb{N}_M^\star = \{1,\dots,M-1\}$.

2. PROBLEM STATEMENT

Let $\mathbf{s}(\mathbf{x})$ denote an unknown B-component image at spatial position $\mathbf{x} \in \mathbb{R}^2$:

$$\mathbf{s}(\mathbf{x}) \triangleq (s^{(1)}(\mathbf{x}),\dots,s^{(B)}(\mathbf{x}))^T. \quad (1)$$

At each sensor b, the spectral component is degraded by the imaging system with impulse response $h^{(b)}(\mathbf{x})$ and, it is also corrupted by an additive noise $n^{(b)}(\mathbf{x})$, which is assumed to be independent of the random process $\mathbf{s}(\mathbf{x})$. The noise

$$\mathbf{n}(\mathbf{x}) \triangleq (n^{(1)}(\mathbf{x}),\dots,n^{(B)}(\mathbf{x}))^T. \quad (2)$$

is a multivariate random field which is assumed to be Gaussian, spatially white, with zero-mean and spectrum density matrix $(\gamma^{(b,b')})_{1\leq b,b'\leq B}$. This means that inter-band correlations may exist.
Therefore, the observations can be expressed as follows:

$$\forall b \in \{1,\dots,B\}, \quad r^{(b)}(\mathbf{x}) = (h^{(b)} * s^{(b)})(\mathbf{x}) + n^{(b)}(\mathbf{x}). \quad (3)$$

For the sake of simplicity, only intra-channel blurring is considered in the previous equation. A deblurring method aims at estimating $\mathbf{s}(\mathbf{x})$ based on the observed vector $\mathbf{r}(\mathbf{x}) \triangleq (r^{(1)}(\mathbf{x}),\dots,r^{(B)}(\mathbf{x}))^T$. A supervised approach assumes that both the blurring kernels $\{h^{(b)}(\mathbf{x})\}_{1\leq b\leq B}$ and the constants $\{(\gamma^{(b,b')})\}_{1\leq b,b'\leq B}$ are known. This is currently a realistic assumption in remote sensing thanks to appropriate calibration procedures [11]. If this assumption does not hold, unsupervised approaches have to estimate the blur and noise parameters from the observed images [15]. Very often, the deconvolution operates in a transform domain, the transform being expected to make the problem easier to model. To this respect, the wavelet domain is considered as a very versatile tool.

3. M-BAND WAVELET TRANSFORM

3.1 Definition

An M-band multiresolution analysis of $\mathrm{L}^2(\mathbb{R})$ is characterized by one scaling function $\psi_0 \in \mathrm{L}^2(\mathbb{R})$ and $(M-1)$ mother wavelets $\psi_m \in \mathrm{L}^2(\mathbb{R})$, $m \in \mathbb{N}_M^\star$. In the Fourier domain, these functions are defined by the so-called scaling equations:

$$\forall m \in \mathbb{N}_M, \qquad \sqrt{M}\widehat{\psi}_m(M\omega) = H_m(\omega)\widehat{\psi}_0(\omega) \tag{4}$$

where $(H_m)_{m\in\mathbb{N}_M}$ are 2π-periodic functions. An orthonormal M-band wavelet basis of $\mathrm{L}^2(\mathbb{R})$ is built when para-unitarity conditions hold:

$$\forall (m,m') \in \mathbb{N}_M^2, \quad \sum_{\mu=0}^{M-1} H_m(p+\frac{\mu}{M})H_{m'}^*(p+\frac{\mu}{M}) = M\delta_{m-m'} \tag{5}$$

It is worth noting that the filter associated to H_0 is low-pass whereas the filters with frequency response $H_1,\ldots,H_{M-2}$ are band-pass and, the filter related to H_{M-1} is high-pass. In this case, cascading M-band para-unitary analysis and synthesis filter banks allows to decompose and to perfectly recover any 1D signal of $\mathrm{L}^2(\mathbb{R})$.
Tensor products of such 1D wavelet system yield the 2D scaling function $\psi_{0,0}(\mathbf{x})$ and M^2-1 wavelet functions $\psi_{m,m'}(\mathbf{x})$ obtained as follows:

$$\forall \mathbf{x} = (x_1,x_2) \in \mathbb{R}^2, \qquad \psi_{0,0}(\mathbf{x}) \stackrel{\triangle}{=} \psi_0(x_1)\psi_0(x_2) \tag{6}$$

$$\forall \mathbf{m} = (m,m') \in {\mathbb{N}_M}^2 \setminus \{(0,0)\}, \quad \psi_{\mathbf{m}}(\mathbf{x}) \stackrel{\triangle}{=} \psi_m(x_1)\psi_{m'}(x_2). \tag{7}$$

In this way, the family $\{\psi_{j,\mathbf{k},\mathbf{m}}\}_{j\in\mathbb{Z},\mathbf{k}\in\mathbb{Z}^2}$ is an orthonormal basis of of $\mathrm{L}^2(\mathbb{R}^2)$ where $\mathbf{m} \in {\mathbb{N}_M}^2 \setminus \{(0,0)\}$ and

$$\forall \mathbf{x} \in \mathbb{R}^2, \qquad \psi_{j,\mathbf{k},\mathbf{m}}(\mathbf{x}) \stackrel{\triangle}{=} M^{j/2}\psi_{\mathbf{m}}(M^j\mathbf{x}-\mathbf{k}). \tag{8}$$

3.2 M-band Meyer wavelets

In the sequel, we will make use of M-band Meyer wavelet decompositions. They involve wavelets of compact support in the frequency domain that have closed-form expressions in this domain. In the dyadic case ($M=2$), the scaling function ψ_0 is a function whose Fourier transform is limited in the frequency domain to $[0,(1+\varepsilon)/2]$ where $\varepsilon \in (0,1/3]$. The corresponding wavelet ψ_1 has a a Fourier transform which is smooth and with compact support within $[(1-\varepsilon)/2, 1+\varepsilon]$ [16]. While the dyadic case is well known, the design of M-band Meyer decompositions has been recently reported in [17].

3.3 Periodized wavelets

A periodized version within the set $[0,1]^2$ of an M-band multiresolution analysis system corresponds to the following *periodic* scaling and wavelet functions $\Psi_{j,\mathbf{k},\mathbf{m}}(\mathbf{x})$:

$$\Psi_{j,\mathbf{k},\mathbf{m}}(\mathbf{x}) \stackrel{\triangle}{=} \sum_{\mathbf{q}\in\mathbb{Z}^2} \psi_{j,\mathbf{k},\mathbf{m}}(\mathbf{x}+\mathbf{q}). \tag{9}$$

Let $j_0 \geq 0$. It has been shown that $\{\Psi_{j_0,\mathbf{k},\mathbf{0}}\}_{j\geq j_0,\mathbf{k}\in\{0,\ldots,M^{j_0}-1\}^2} \cup \{\Psi_{j,\mathbf{k},\mathbf{m}}\}_{j\geq j_0,\mathbf{k}\in\{0,\ldots,M^j-1\}^2,\mathbf{m}\neq\mathbf{0}}$ is an orthonormal basis of the space of periodic functions in $L^2([0,1]^2)$. Hence, the wavelet coefficients $g_{j,\mathbf{m}}$ of any periodic function g in $\mathrm{L}^2([0,1]^2)$ are given by:

$$g_{j,\mathbf{m}}(\mathbf{k}) = \int_0^1\int_0^1 g(\mathbf{x})\Psi_{j,\mathbf{k},\mathbf{m}}(\mathbf{x})d\mathbf{x}. \tag{10}$$

4. COMBINING WAVELET AND FOURIER TRANSFORMS FOR DECONVOLUTION

The approach developed in [13, 18] judiciously combines Fourier analysis with a dyadic Meyer wavelet expansion. In what follows, we will generalize this approach by considering multicomponent images analyzed through an M-band decomposition. Each spectral component $s^{(b)}$ is viewed as a periodic function in $\mathrm{L}^2([0,1]^2)$ whose Fourier coefficients $S^{(b)}(\mathbf{p})$ are given by:

$$\forall \mathbf{p} \in \mathbb{Z}^2, \quad S^{(b)}(\mathbf{p}) \stackrel{\triangle}{=} \int_0^1\int_0^1 s^{(b)}(\mathbf{x})\exp(-2\pi\imath\mathbf{x}^T\mathbf{p})d\mathbf{x}. \tag{11}$$

In the frequency domain, Eq. (3) becomes:

$$\forall b \in \{1,\ldots,B\}, \qquad R^{(b)}(\mathbf{p}) = U^{(b)}(\mathbf{p}) + N^{(b)}(\mathbf{p}), \tag{12}$$

where

$$U^{(b)}(\mathbf{p}) \stackrel{\triangle}{=} H^{(b)}(\mathbf{p})S^{(b)}(\mathbf{p}), \tag{13}$$

and the Fourier coefficients $S^{(b)}(\mathbf{p})$ and $N^{(b)}(\mathbf{p})$ are obtained by expressions similar to Eq. (11). It must be pointed out that Eq. (13) actually corresponds to an approximation of the 2D convolution in Eq. (3) by a periodic convolution (this problem can be solved by making use of zero-padding techniques). Besides, Plancherel's formula reduces to:

$$\int_0^1\int_0^1 s^{(b)}(\mathbf{x})\Psi_{j,\mathbf{k},\mathbf{m}}(\mathbf{x})d\mathbf{x} = \sum_{\mathbf{p}} S^{(b)}(\mathbf{p})\widehat{\Psi}_{j,\mathbf{k},\mathbf{m}}^*(\mathbf{p}), \tag{14}$$

where $\widehat{\Psi}_{j,\mathbf{k},\mathbf{m}}(\mathbf{p})$ is a Fourier coefficient of $\Psi_{j,\mathbf{k},\mathbf{m}}(\mathbf{x})$, which is also equal to the Fourier transform of $\psi_{j,\mathbf{k},\mathbf{m}}(\mathbf{x})$ at frequency $\mathbf{p}$. By combining Equations (10) and (14), the wavelet coefficients can be obtained as follows:

$$s_{j,\mathbf{m}}^{(b)}(\mathbf{k}) = \sum_{\mathbf{p}\in\mathscr{C}_{j,\mathbf{m}}} S^{(b)}(\mathbf{p})\widehat{\Psi}_{j,\mathbf{k},\mathbf{m}}^*(\mathbf{p}), \tag{15}$$

where $\mathscr{C}_{j,\mathbf{m}} \stackrel{\triangle}{=} \{\mathbf{p}\in\mathbb{Z}^2 : \widehat{\Psi}_{j,\mathbf{k},\mathbf{m}}(\mathbf{p}) \neq 0\}$. It is worth pointing out that $\mathscr{C}_{j,\mathbf{m}}$ does not depend on $\mathbf{k}$. This is equivalent to:

$$s_{j,\mathbf{m}}^{(b)}(\mathbf{k}) = \sum_{\mathbf{p}\in\mathscr{C}_{j,\mathbf{m}}} \frac{U^{(b)}(\mathbf{p})}{H^{(b)}(\mathbf{p})}\widehat{\Psi}_{j,\mathbf{k},\mathbf{m}}^*(\mathbf{p}), \tag{16}$$

provided that, for all $\mathbf{p} \in \mathscr{C}_{j,\mathbf{m}}$, $H^{(b)}(\mathbf{p}) \neq 0$. At this point, it is important to note that it appears preferable to use frequency bandlimited wavelets such as M-band Meyer wavelets. Indeed, in this case, the cardinality of $\mathscr{C}_{j,\mathbf{m}}$ is drastically reduced and the above condition is not fulfilled only by the zeros of $H^{(b)}$ belonging to the frequency support of $\widehat{\Psi}_{j,\mathbf{k},\mathbf{m}}(\mathbf{p})$.
The detail coefficients cannot be recovered by the latter equation since the sequence $U^{(b)}(\mathbf{p})$ is not observable. In [13], it is proposed to use $R^{(b)}(\mathbf{p})$ as an unbiased estimator of $U^{(b)}(\mathbf{p})$. As a result, the so-called Waved estimator $\hat{s}_{j,\mathbf{m}}^{(b)}(\mathbf{k})$ of $s_{j,\mathbf{m}}^{(b)}(\mathbf{k})$ is obtained:

$$\hat{s}_{j,\mathbf{m}}^{(b)}(\mathbf{k}) = \sum_{\mathbf{p}\in\mathscr{C}_{j,\mathbf{m}}} \frac{R^{(b)}(\mathbf{p})}{H^{(b)}(\mathbf{p})}\widehat{\Psi}_{j,\mathbf{k},\mathbf{m}}^*(\mathbf{p}). \tag{17}$$

Then, it remains to improve the performance of such a coarse estimator $\hat{s}_{j,\mathbf{m}}^{(b)}(\mathbf{k})$ through an additional denoising. In [13], for an appropriate set of target functions, an asymptotically near-optimal estimator (in the sense of the mean square error) $\tilde{s}_{j,\mathbf{m}}^{(b)}(\mathbf{k})$ is derived through hard-thresholding by level-dependent thresholds $\lambda_{j,\mathbf{m}}$:

$$\lambda_{j,\mathbf{m}} = \lambda\frac{\log(L)}{2\sqrt{L}}\left(\gamma^{(b,b)}|\mathscr{C}_{j,\mathbf{m}}|^{-1}\sum_{\mathbf{p}\in\mathscr{C}_{j,\mathbf{m}}}|H^{(b)}(\mathbf{p})|^{-2}\right)^{1/2}, \tag{18}$$

where L is the whole number of pixels in each spectral component, $|\mathscr{C}_{j,\mathbf{m}}|$ denotes the cardinality of $\mathscr{C}_{j,\mathbf{m}}$ and λ is a constant factor. It is worth pointing out that the wavelet shrinkage is operated from the coarsest scale j_0 up to a finest scale j_1. The latter is related to the degree of ill-posedness of the blurring kernel $H^{(b)}(\mathbf{p})$ [13]. The main contribution of our work consists in proposing an improved method for denoising all the coefficients $\{\tilde{s}^{(b)}_{j,\mathbf{m}}(\mathbf{k})\}_{b=1}^{B}$ by adopting a *multivariate* approach.

5. STATISTICS OF THE WAVED ESTIMATOR

In order to denoise $\tilde{s}^{(b)}_{j,\mathbf{m}}(\mathbf{k})$, it is useful to derive the statistics of this estimator. First of all, the Gaussianity of the noise and the linearity of the estimator ensures the Gaussianity of $e^{(b)}_{j,\mathbf{m}}(\mathbf{k}) \stackrel{\triangle}{=} \tilde{s}^{(b)}_{j,\mathbf{m}}(\mathbf{k}) - s^{(b)}_{j,\mathbf{m}}(\mathbf{k})$. Besides, it is easy to show that $\tilde{s}^{(b)}_{j,\mathbf{m}}(\mathbf{k})$ is an unbiased estimator since:

$$\begin{aligned} E[\tilde{s}^{(b)}_{j,\mathbf{m}}(\mathbf{k})] &= \sum_{\mathbf{p}\in\mathscr{C}_{j,\mathbf{m}}} \frac{E[R^{(b)}(\mathbf{p})]}{H^{(b)}(\mathbf{p})} \widehat{\Psi}^{*}_{j,\mathbf{k},\mathbf{m}}(\mathbf{p}) \\ &= \sum_{\mathbf{p}\in\mathscr{C}_{j,\mathbf{m}}} \frac{H^{(b)}(\mathbf{p})E[S^{(b)}(\mathbf{p})]}{H^{(b)}(\mathbf{p})} \widehat{\Psi}^{*}_{j,\mathbf{k},\mathbf{m}}(\mathbf{p}) \\ &= E[s^{(b)}_{j,\mathbf{m}}(\mathbf{k})]. \end{aligned} \tag{19}$$

The mean square estimation error $\gamma^{(b,b)}_{j,\mathbf{m}}$ is given by:

$$\begin{aligned} \gamma^{(b,b)}_{j,\mathbf{m}} &\stackrel{\triangle}{=} E[\left(\tilde{s}^{(b)}_{j,\mathbf{m}}(\mathbf{k}) - s^{(b)}_{j,\mathbf{m}}(\mathbf{k})\right)^2] \\ &= \sum_{\mathbf{p}\in\mathscr{C}_{j,\mathbf{m}}} E[|N^{(b)}(\mathbf{p})|^2] \left| \frac{\widehat{\Psi}_{j,\mathbf{k},\mathbf{m}}(\mathbf{p})}{H^{(b)}(\mathbf{p})} \right|^2 \\ &= \gamma^{(b,b)} \sum_{\mathbf{p}\in\mathscr{C}_{j,\mathbf{m}}} \left| \frac{\widehat{\Psi}_{j,\mathbf{0},\mathbf{m}}(\mathbf{p})}{H^{(b)}(\mathbf{p})} \right|^2. \end{aligned} \tag{20}$$

The cross correlation $\gamma^{(b,b')}_{j,\mathbf{m}}$ of the estimation errors for any pair of components (b,b') at the same location $\mathbf{k}$ can be calculated in a similar way:

$$\begin{aligned} \gamma^{(b,b')}_{j,\mathbf{m}} &\stackrel{\triangle}{=} E[\left(\tilde{s}^{(b)}_{j,\mathbf{m}}(\mathbf{k}) - s^{(b)}_{j,\mathbf{m}}(\mathbf{k})\right)\left(\tilde{s}^{(b')}_{j,\mathbf{m}}(\mathbf{k}) - s^{(b')}_{j,\mathbf{m}}(\mathbf{k})\right)] \\ &= \gamma^{(b,b')} \sum_{\mathbf{p}\in\mathscr{C}_{j,\mathbf{m}}} \frac{|\widehat{\Psi}_{j,\mathbf{0},\mathbf{m}}(\mathbf{p})|^2}{H^{(b)}(\mathbf{p})H^{(b')}(\mathbf{p})^*}. \end{aligned} \tag{21}$$

It is also worth pointing out that $s^{(b)}_{j,\mathbf{m}}(\mathbf{k})$ and $e^{(b)}_{j,\mathbf{m}}(\mathbf{k})$ are decorrelated since:

$$E[s^{(b)}_{j,\mathbf{m}}(\mathbf{k})\tilde{s}^{(b)}_{j,\mathbf{m}}(\mathbf{k})] = E[s^{(b)}_{j,\mathbf{m}}(\mathbf{k})^2]. \tag{22}$$

Indeed, the calculation of $E[s^{(b)}_{j,\mathbf{m}}(\mathbf{k})\tilde{s}^{(b)}_{j,\mathbf{m}}(\mathbf{k})]$ yields to:

$$\begin{aligned} E[s^{(b)}_{j,\mathbf{m}}(\mathbf{k})\tilde{s}^{(b)}_{j,\mathbf{m}}(\mathbf{k})] &= \sum_{\mathbf{p},\mathbf{p}'\in\mathscr{C}_{j,\mathbf{m}}} \frac{E[S^{(b)}(\mathbf{p})R^{(b)}(\mathbf{p}')^*]}{H^{(b)}(\mathbf{p}')^*} \\ &\qquad \widehat{\Psi}^{*}_{j,\mathbf{k},\mathbf{m}}(\mathbf{p})\widehat{\Psi}_{j,\mathbf{k},\mathbf{m}}(\mathbf{p}') \\ &= \sum_{\mathbf{p},\mathbf{p}'\in\mathscr{C}_{j,\mathbf{m}}} E[S^{(b)}(\mathbf{p})S^{(b)}(\mathbf{p}')^*] \\ &\qquad \widehat{\Psi}^{*}_{j,\mathbf{k},\mathbf{m}}(\mathbf{p})\widehat{\Psi}_{j,\mathbf{k},\mathbf{m}}(\mathbf{p}') \\ &= E[s^{(b)}_{j,\mathbf{m}}(\mathbf{k})^2]. \end{aligned} \tag{23}$$

6. PROPOSED MULTICHANNEL WAVED ESTIMATOR

6.1 Motivation

The multivariate approach consists in estimating *jointly* all the B wavelet coefficients $s^{(b)}_{j,\mathbf{m}}(\mathbf{k})$ from all the B waved estimators $\tilde{s}^{(b)}_{j,\mathbf{m}}(\mathbf{k})$. To this purpose, we define the following B-dimensional vectors: $\mathbf{s}_{j,\mathbf{m}}(\mathbf{k}) \stackrel{\triangle}{=} (s^{(1)}_{j,\mathbf{m}}(\mathbf{k}),\ldots,s^{(B)}_{j,\mathbf{m}}(\mathbf{k}))^T$ and, $\tilde{\mathbf{s}}_{j,\mathbf{m}}(\mathbf{k}) \stackrel{\triangle}{=} (\tilde{s}^{(1)}_{j,\mathbf{m}}(\mathbf{k}),\ldots,\tilde{s}^{(B)}_{j,\mathbf{m}}(\mathbf{k}))^T$. By defining the noise vector $\mathbf{e}_{j,\mathbf{m}}(\mathbf{k})$ as:

$$\tilde{\mathbf{s}}_{j,\mathbf{m}}(\mathbf{k}) = \mathbf{s}_{j,\mathbf{m}}(\mathbf{k}) + \mathbf{e}_{j,\mathbf{m}}(\mathbf{k}), \tag{24}$$

we get an additive noise observation model. From Section 5, it appears that the unknown vector $\mathbf{s}_{j,\mathbf{m}}(\mathbf{k})$ is embedded in the zero-mean *multivariate* Gaussian noise $\mathbf{e}_{j,\mathbf{m}}(\mathbf{k})$ with $\gamma^{(b,b')}_{j,\mathbf{m}}$ as the (b,b') generic element of its autocovariance matrix $\mathbf{\Gamma}^{(e)}_{j,\mathbf{m}}$. Therefore, it is possible to apply a robust estimator of the whole *vector* $\mathbf{s}_{j,\mathbf{m}}(\mathbf{k})$ that can exploit the intercomponent correlations. In a recent work [3], we have envisaged two multivariate denoising methods: a MAP estimation and a more robust one built on Stein's principle operating on dyadic decompositions. In the sequel, we will extend them to the M-band wavelet restoration problem.

6.2 Multivariate MAP

Concerning the MAP method, a prior Bernouilli-Gaussian (BG) distribution $p_{j,\mathbf{m}}$ is considered so as to reflect the sparseness of $\mathbf{s}_{j,\mathbf{m}}(\mathbf{k})$ as well as the statistical dependencies existing between the B components:

$$\forall \mathbf{u}\in\mathbb{R}^B, \quad p_{j,\mathbf{m}}(\mathbf{u}) = (1-\varepsilon_{j,\mathbf{m}})\delta(\mathbf{u}) + \varepsilon_{j,\mathbf{m}} g_{\mathbf{0},\mathbf{\Gamma}^{(s)}_{j,\mathbf{m}}}(\mathbf{u}), \tag{25}$$

where δ is the Dirac distribution, $g_{\mathbf{0},\mathbf{\Gamma}^{(s)}_{j,\mathbf{m}}}$ is the multivariate Gaussian $\mathscr{N}(\mathbf{0},\mathbf{\Gamma}^{(s)}_{j,\mathbf{m}})$ probability density and $\varepsilon_{j,\mathbf{m}}\in[0,1]$ is the mixture parameter. In tandem with this mixed distribution we use an independent binary random (hidden) variables $q_{j,\mathbf{m}}(\mathbf{k})$ such that:

$$\begin{array}{rcl} p(\mathbf{s}_{j,\mathbf{m}}(\mathbf{k})/q_{j,\mathbf{m}}(\mathbf{k})=0) &=& \delta(\mathbf{s}_{j,\mathbf{m}}(\mathbf{k})) \\ p(\mathbf{s}_{j,\mathbf{m}}(\mathbf{k})/q_{j,\mathbf{m}}(\mathbf{k})=1) &=& g_{\mathbf{0},\mathbf{\Gamma}^{(s)}_{j,\mathbf{m}}}(\mathbf{s}_{j,\mathbf{m}}(\mathbf{k})) \end{array}. \tag{26}$$

Only when $q_{j,\mathbf{m}}(\mathbf{k})=1$, the associated wavelet coefficient vector carries useful information. Besides, the Gaussianity of the noise allows to express the conditional probabilities:

$$\left\{ \begin{array}{rcl} p(\tilde{\mathbf{s}}_{j,\mathbf{m}}(\mathbf{k})/q_{j,\mathbf{m}}(\mathbf{k})=0) &=& g_{\mathbf{0},\mathbf{\Gamma}^{(e)}_{j,\mathbf{m}}}(\tilde{\mathbf{s}}_{j,\mathbf{m}}(\mathbf{k})) \\ p(\tilde{\mathbf{s}}_{j,\mathbf{m}}(\mathbf{k})/q_{j,\mathbf{m}}(\mathbf{k})=1) &=& g_{\mathbf{0},\mathbf{\Gamma}^{(e)}_{j,\mathbf{m}}+\mathbf{\Gamma}^{(s)}_{j,\mathbf{m}}}(\tilde{\mathbf{s}}_{j,\mathbf{m}}(\mathbf{k})) \end{array} \right. . \tag{27}$$

Consequently, the denoising problem reduces to a classical problem in estimation theory. However, because of the singularity of the a posteriori distribution $p_{\mathbf{s}_{j,\mathbf{m}}}(\mathbf{u}/\tilde{\mathbf{s}}_{j,\mathbf{m}}(\mathbf{k}))$ due to the Dirac distribution, the MAP estimate takes a degenerate form. This is why the $q_{j,\mathbf{m}}(\mathbf{k})$ are estimated before the computation of the MAP estimate $\hat{\mathbf{s}}^{(\mathrm{MAP})}_{j,\mathbf{m}}(\mathbf{k})$. More precisely, the Bayesian estimate $\hat{q}_{j,\mathbf{m}}(\mathbf{k})=1$ of $q_{j,\mathbf{m}}(\mathbf{k})$ satisfies:

$$\hat{q}_{j,\mathbf{m}}(\mathbf{k}) = \left\{ \begin{array}{ll} 1 & \text{if } \tilde{\mathbf{s}}_{j,\mathbf{m}}(\mathbf{k})^T \mathbf{M}_{j,\mathbf{m}} \tilde{\mathbf{s}}_{j,\mathbf{m}}(\mathbf{k}) > \chi_{j,\mathbf{m}}, \\ 0 & \text{otherwise} \end{array} \right. \tag{28}$$

where $\mathbf{M}_{j,\mathbf{m}} = (\mathbf{\Gamma}^{(e)}_{j,\mathbf{m}})^{-1} - (\mathbf{\Gamma}^{(s)}_{j,\mathbf{m}} + \mathbf{\Gamma}^{(e)}_{j,\mathbf{m}})^{-1}$ and, the threshold $\chi_{j,\mathbf{m}}$ is given by:

$$\chi_{j,\mathbf{m}} = 2\ln\left(\frac{1-\varepsilon_{j,\mathbf{m}}}{\varepsilon_{j,\mathbf{m}}}\right) + \ln\left(\frac{|\,\mathbf{\Gamma}^{(s)}_{j,\mathbf{m}} + \mathbf{\Gamma}^{(e)}_{j,\mathbf{m}}\,|}{|\,\mathbf{\Gamma}^{(e)}_{j,\mathbf{m}}\,|}\right). \tag{29}$$

The corresponding MAP estimator is easily deduced:

$$\hat{\mathbf{s}}_{j,\mathbf{m}}^{(\mathrm{MAP})}(\mathbf{k}) = \begin{cases} \mathbf{Q}_{j,\mathbf{m}}\tilde{\mathbf{s}}_{j,\mathbf{m}}(\mathbf{k}) & \text{if } \hat{q}_{j,\mathbf{m}}(\mathbf{k}) = 1 \\ \mathbf{0} & \text{otherwise} \end{cases}, \quad (30)$$

where $\mathbf{Q}_{j,\mathbf{m}} \triangleq \mathbf{\Gamma}_{j,\mathbf{m}}^{(s)}(\mathbf{\Gamma}_{j,\mathbf{m}}^{(s)} + \mathbf{\Gamma}_{j,\mathbf{m}}^{(e)})^{-1}$ [3].

6.3 Stein's estimator

It is possible to build another estimator $\hat{\mathbf{s}}_{j,\mathbf{m}}^{(\mathrm{Stein})}$ that takes into account the BG model mismatch. More precisely, we replace the MAP estimator by $E[\mathbf{s}_{j,\mathbf{m}}/\tilde{\mathbf{s}}_{j,\mathbf{m}}]$ which is the optimal Bayesian estimator for a quadratic cost:

$$E[\mathbf{s}_{j,\mathbf{m}}/\tilde{\mathbf{s}}_{j,\mathbf{m}}] = \gamma_{\varepsilon_{j,\mathbf{m}}}(\tilde{\mathbf{s}}_{j,\mathbf{m}})\mathbf{Q}_{j,\mathbf{m}}\tilde{\mathbf{s}}_{j,\mathbf{m}}, \quad (31)$$

$$\text{where } \gamma_{\varepsilon_{j,\mathbf{m}}} \triangleq \frac{\varepsilon_{j,\mathbf{m}} g_{\mathbf{0},\mathbf{\Gamma}_{j,\mathbf{m}}^{(s)}+\mathbf{\Gamma}_{j,\mathbf{m}}^{(e)}}}{\varepsilon_{j,\mathbf{m}} g_{\mathbf{0},\mathbf{\Gamma}_{j,\mathbf{m}}^{(s)}+\mathbf{\Gamma}_{j,\mathbf{m}}^{(e)}} + (1-\varepsilon_{j,\mathbf{m}}) g_{\mathbf{0},\mathbf{\Gamma}_{j,\mathbf{m}}^{(e)}}} \quad (32)$$

We propose to use an estimator $\hat{\mathbf{s}}_{j,\mathbf{m}}^{(\mathrm{Stein})}$ whose structure is given by Eqs. (31)-(32). But, instead of deducing $\mathbf{Q}_{j,\mathbf{m}}$ and $\varepsilon_{j,\mathbf{m}}$ from the BG prior, the latter are adjusted so as to minimize the quadratic risk $\mathscr{E}_{j,\mathbf{m}} = E[\|\mathbf{s}_{j,\mathbf{m}} - \hat{\mathbf{s}}_{j,\mathbf{m}}^{(\mathrm{Stein})}\|^2]$. A closed form expression of $R_{j,\mathbf{m}}$ can be derived thanks to Stein's formula yielding the cost function:

$$\tilde{\mathscr{E}}_{j,\mathbf{m}} = -\mathrm{tr}(\mathbf{B}_{j,\mathbf{m}}(\mathbf{A}_{j,\mathbf{m}})^{-1}\mathbf{B}_{j,\mathbf{m}}^T), \quad (33)$$

$$\text{with } \mathbf{A}_{j,\mathbf{m}} \triangleq E[\gamma_{\varepsilon_{j,\mathbf{m}}}^2(\tilde{\mathbf{s}}_{j,\mathbf{m}})\tilde{\mathbf{s}}_{j,\mathbf{m}}(\tilde{\mathbf{s}}_{j,\mathbf{m}})^T]. \quad (34)$$

$$\mathbf{B}_{j,\mathbf{m}} \triangleq E[\gamma_{\varepsilon_{j,\mathbf{m}}}(\tilde{\mathbf{s}}_{j,\mathbf{m}})\tilde{\mathbf{s}}_{j,\mathbf{m}}(\tilde{\mathbf{s}}_{j,\mathbf{m}})^T] - \mathbf{\Gamma}_{j,\mathbf{m}}^{(e)}(E[\gamma_{\varepsilon_{j,\mathbf{m}}}(\tilde{\mathbf{s}}_{j,\mathbf{m}})]\mathbf{I} + E[\nabla\gamma_{\varepsilon_{j,\mathbf{m}}}(\tilde{\mathbf{s}}_{j,\mathbf{m}})(\tilde{\mathbf{s}}_{j,\mathbf{m}})^T])$$

So, the minimization of $R_{j,\mathbf{m}}$ amounts to the optimization of a function of the single variable $\varepsilon_{j,\mathbf{m}} \in [0,1]$ since it is easy to check that the corresponding optimal $\mathbf{Q}_{j,\mathbf{m}}$ is $\mathbf{B}_{j,\mathbf{m}}(\mathbf{A}_{j,\mathbf{m}})^{-1}$.

A further improvement consists in envisaging a hybrid scheme that allows to handle unreliable values of the risk especially in very noisy environments. For instance, the data $\tilde{s}_{j,\mathbf{m}}^{(b)}$ are considered as too noisy if the power level of the "clean" data falls below a given threshold $\lambda_{j,\mathbf{m}}^{(b)}$ and, then, they are discarded from the estimation of the risk as described in [2]. In this case, the SURE componentwise estimator is applied.

7. EXPERIMENTAL RESULTS

In our experiments, we have used SPOT multispectral images of size 512×512. These images have been degraded by considering several blurring kernels and, adding realizations of a zero-mean Gaussian noise. Our preliminary simulations were concerned with spectrally and spatially white noise. The additive noise variance $\gamma^{(b,b)}$ is chosen so that the averaged blurred signal to noise ratio *BSNR* reaches a target value:

$$BSNR \triangleq \frac{1}{B}\sum_{b=1}^{B} BSNR^{(b)} \quad (35)$$

$$\text{with } BSNR^{(b)} \triangleq 10\log_{10}\left(\frac{\| h^{(b)} * s^{(b)} - E[h^{(b)} * s^{(b)}] \|^2}{L\gamma^{(b,b)}}\right). \quad (36)$$

The involved filters of the M-band Meyer's wavelet are implemented according to the procedure described in [17]. Monte-Carlo simulations have been conducted, the performance of a deconvolution method being assessed by the averaged Improvement in Signal to Noise Ratio *ISNR*:

$$ISNR \triangleq \frac{1}{B}\sum_{b=1}^{B} 10\log_{10}\left(\frac{E[(s^{(b)} - r^{(b)})^2]}{E[(s^{(b)} - \hat{s}^{(b)})^2]}\right). \quad (37)$$

For a fair comparison, we have also made comparisons with up-to-date wavelet-based restoration methods. All of them are separately applied to each spectral component, employing their own setup. The Waved, the Stein and the MAP estimators are derived from a *non redundant* two-band Meyer's WT ($M = 2$). The Forward method uses Daubechies WT. Thanks to the "cycle-spinning" strategy, the resulting representation is spatially invariant but it is also redundant. The Forward estimator has been applied with a fixed value of the regularization parameter. The number of resolution levels is set to $J = 2$. We have also tested the Wiener filter (with the version provided in [12]). Table 1 provides the *ISNR* achieved by the different considered techniques for several values of the *BSNR*. As expected, by taking into account the intercomponent similarities, our two methods almost always outperform the benchmarked ones. By avoiding a prior model mismatch, $\hat{\mathbf{s}}_{j,\mathbf{m}}^{(\mathrm{Stein})}$ exhibits better performance than $\hat{\mathbf{s}}_{j,\mathbf{m}}^{(\mathrm{MAP})}$. It is worthwile noticing that if we use a redundant translation invariant version of the WT (like the forward method), higher values of the *ISNR* should be achieved by our estimators. Table 2 gives the resulting *ISNR* for different sizes of the blurring kernel when the *BSNR* is equal to 25 dB. It indicates that the behavior of the considered techniques remains the same: $\hat{\mathbf{s}}^{(\mathrm{Stein})}$ produces the best results whatever the support of the blurring mask is. For instance, it yields a gain of 0.63 dB in terms of *ISNR* over the Forward method for the "Tunis" image.

Figure 1 displays the degraded component XS3 of the "Kairouan" image that depicts a rural area ($b = 3$). Figure 2 shows the restored component using $\hat{\mathbf{s}}^{(\mathrm{Stein})}$. The overall visual quality is good even around the edges of the objects in the scene. Fine details such as the roads are clearly visible.

8. CONCLUSIONS

We have proposed a restoration method that exploits crosschannel similarities in multicomponent images. This approach was shown to be very competitive w.r.t. existing wavelet-based methods. Several directions can be investigated to extend this work. In particular, it would be interesting to take into account interscale dependencies between spectral components in addition to intrascale ones. An improved structure of the waved estimator is also under investigation.

REFERENCES

[1] I. Pitas, A. Venetsanopoulos, *Nonlinear digital filters*, Kluwer, Dodrecht, 1990.

[2] D. L. Donoho and I. M. Johnstone, "Adapting to unknown smoothness via wavelet shrinkage," *J. of the Amer. Stat. Ass.*, vol. 90, pp. 1200-1224, 1995.

[3] A. Benazza-Benyahia and J. C. Pesquet, "Building Robust Wavelet Estimators for Multicomponent Images Using Stein's Principle, " *IEEE Image Processing Transactions*, vol. 14, pp. 1814-1830, Nov. 2005.

[4] G. Demoment, "Image reconstruction and restoration: overview of common estimation structure and problems," *IEEE Trans. on Speech, Signal Processing*, vol. 37, pp. 2024-2036, Dec. 1989.

[5] J. Idier, "Convex half-quadratic criteria and interacting auxilary variables for image restoration," *IEEE Trans. on Image Processing*, vol. 10, pp. 1001-1009, July 2001.

[6] A. K. Katsaggelos, *Digital image restoration*, Springer-Verlag, New-York, 1991.

[7] B. R. Hunt and O. Kübler, "Karhunen-Loeve multispectral image restoration, part I: theory," *IEEE Trans. Acoustics, Speech, and Signal Processing*, vol. 32, pp. 592-600, June 1984.

[8] N. P. Galatsanos, and R. T Chin, "Restoration of color images by multichannel Kalman filtering," *IEEE Trans. on Image Processing*, vol. 39, pp. 2237-2252, 1991.

[9] N. P. Galatsanos, and R. T. Chin, "Digital restoration of MC images," *IEEE Trans Acoustics , Speech, and Signal Processing*, vol. 37, pp. 415-421, Mar. 1989.

[10] F. Abramovich, and B. W. Silverman, "Wavelet decomposition approaches to statistical inverse problems," *Biometrika*, vol. 85, pp. 115-129, 1998.

[11] J. Kalifa, S. Mallat, and B. Rougé, "Deconvolution by thresholding in mirror wavelet bases," *IEEE Trans. Image Processing*, vol. 12, pp. 446-457, Apr. 2003.

[12] R. Neelamani, H. Choi, and R. Baraniuk, "Forward: Fourier-wavelet regularized deconvolution for ill-conditioned systems," *IEEE Trans. on Signal Processing*, vol. 52, pp. 418-433, Feb. 2004.

[13] I. M. Johnstone, G. Kerkyacharian, D. Picard, and M. Raimondo, "Wavelet deconvolution in a periodic setting," *J.R. Statistic. Soc. B*, vol. 66, part 3, pp. 547-573, 2004.

[14] I. Daubechies, M. Defrise, and C. De Mol, "An iterative thresholding algorithm for linear inverse problems with a sparsity constraint," *Comm. Pure Appl. Math.*, vol. 57, pp. 1413–1457, 2004.

[15] A. Jalobeanu, L. Blanc-Féraud, and J. Zerubia, "Hyperparameter estimation for satellite image restoration using a MCMC maximum likelihood method," *Pattern Recognition*, vol. 35, pp. 341-352, 2002.

[16] Y. Meyer, *Ondelettes et Opérateurs-I*, Hermann, 1990.

[17] B. Tennant, and R. M. Rao, "Solution to the orthogonal *M*-channel bandlimited wavelet bases," in *Proc. of the ICASSP*, Honk-Kong, China, April 6-10, 2003.

[18] D. L. Donoho and M. E. Raimondo, "A fast wavelet algorithm for image deblurring," *ANZIAM Journal*, vol. 14, pp. C29-C46, Mar. 2005.

Table 1: Resulting *ISNR* (in dB) of the tested restoration methods. The size of the blurring kernel is respectively 5×5 for the image "Tunis" and, 9×9 for the image "Kairouan".

(a) Tunis

BSNR	Waved	Wiener	Forward	$\hat{\mathbf{s}}_{j,\mathbf{m}}^{(\mathrm{MAP})}$	$\hat{\mathbf{s}}_{j,\mathbf{m}}^{(\mathrm{Stein})}$
15	5.2141	3.6922	8.4673	8.6445	**9.0877**
25	8.9609	12.3754	14.6004	14.6835	**15.1998**
35	16.5929	22.2259	23.1091	22.8219	**23.2760**
45	7.3894	32.2219	**32.5455**	32.0887	32.4703

(b) Kairouan

BSNR	Waved	Wiener	Forward	$\hat{\mathbf{s}}_{j,\mathbf{m}}^{(\mathrm{MAP})}$	$\hat{\mathbf{s}}_{j,\mathbf{m}}^{(\mathrm{Stein})}$
15	4.6771	4.7174	8.2187	8.5040	**9.0409**
25	12.7939	17.7246	18.8378	18.4001	**19.2918**
35	21.5830	27.6886	27.8075	27.1757	**27.9595**
45	33.3587	37.6893	37.7210	37.4699	**37.7191**

Table 2: Resulting *ISNR* (in dB) of the tested restoration methods according to the size of the square blurring kernel. The *BSNR* is fixed to 25 dB.

(a) Tunis

Size	Waved	Wiener	Forward	$\hat{\mathbf{s}}_{j,\mathbf{m}}^{(\mathrm{MAP})}$	$\hat{\mathbf{s}}_{j,\mathbf{m}}^{(\mathrm{Stein})}$
3	6.6079	9.8321	12.1874	12.2750	**12.8075**
5	8.9609	12.3754	14.6004	14.6835	**15.1998**
7	10.1592	13.5779	15.7497	15.8263	**16.3282**
9	10.8524	14.3054	16.4363	16.5187	**17.0117**

(b) Kairouan

Size	Waved	Wiener	Forward	$\hat{\mathbf{s}}_{j,\mathbf{m}}^{(\mathrm{MAP})}$	$\hat{\mathbf{s}}_{j,\mathbf{m}}^{(\mathrm{Stein})}$
3	8.6020	13.2715	14.6208	14.1821	**15.1188**
5	6.7308	11.3184	12.9947	12.5551	**13.1552**
5	10.8743	15.7067	16.9240	16.5194	**17.4180**
7	12.0780	16.9460	18.1020	17.6800	**18.5703**
9	12.7939	17.7246	18.8378	18.4001	**19.2918**

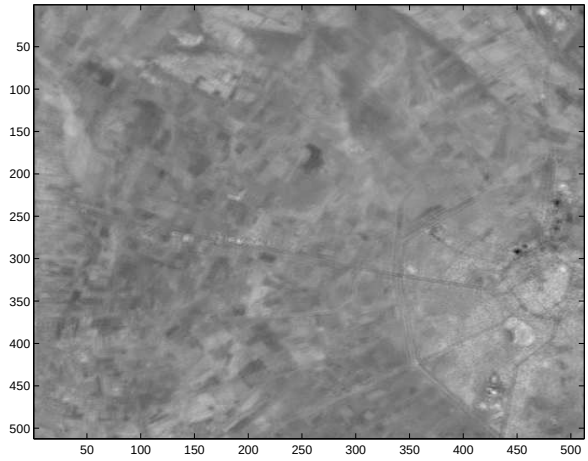

Figure 1: "Kairouan": third channel XS3 degraded by a blurring kernel of size 9×9, $BSNR^{(3)} = 25$ dB.

Figure 2: "Kairouan": third channel XS3 restored by $\hat{s}^{(\mathrm{Stein})}$, $ISNR = 19.2918$ dB.